Discovery of a new selective inhibitor of A Disintegrin And Metalloprotease 10 (ADAM-10) able to reduce the shedding of NKG2D ligands in Hodgkin's lymphoma cell models.

Caterina Camodeca,[a] Elisa Nuti,[b] Livia Tepshi,[b,c] Silvia Boero,[d] Tiziano Tuccinardi,[b] Enrico A. Stura,[c] Alessandro Poggi,[d] Maria Raffaella Zocchi,[a] and Armando Rossello[b*]

[a] Division of Immunology, Transplants and Infectious Diseases, San Raffaele Scientific Institute, 20132 Milan, Italy.

[b] Dipartimento di Farmacia, Università di Pisa, via Bonanno 6, 56126 Pisa, Italy.

[c] CEA, iBiTec-S, Service d'Ingenierie Moleculaire des Proteines, CE-Saclay, 91191 Gif sur Yvette Cedex, France.

[d] Unit of Molecular Oncology and Angiogenesis, IRCCS AOU San Martino-IST, 16132 Genoa, Italy.

Abstract: Hodgkin's lymphoma (HL) is the most common malignant lymphoma in young adults in the western world. This disease is characterized by an overexpression of ADAM-10 with increased release of NKG2D ligands, involved in an impaired immune response against tumor cells. We designed and synthesized two new ADAM-10 selective inhibitors, **2** and **3** based on previously published ADAM-17 selective inhibitor **1**. The most promising compound was the thiazolidine derivative **3**, with nanomolar activity for ADAM-10, high selectivity over ADAM-17 and MMPs and good efficacy in reducing the shedding of NKG2D ligands (MIC-B and ULBP3) in three different HL cell lines at non-toxic doses. Molecular modeling studies were used to drive the design and X-ray crystallography studies were carried out to explain the selectivity of **3** for ADAM-10 over MMPs.

Keywords:
Hodgkin's lymphoma
NKG2D-L
ADAM-10 inhibitors
Sulfonamido-based hydroxamates

Abbreviations: HL, Hodgkin's lymphoma; ADAM, a disintegrin and metalloproteinase; ALCAM, activated leukocyte cell adhesion molecule; EOC, epithelial ovarian cancer; NK, natural killer; NKG2D, natural killer group-2; ULBP, unique long 16 binding proteins; MHC, major histocompatibility complex; MIC-A/B, major histocompatibility complex class I chain-related proteins A and B; SN, supernatants; EDC, N-(3-Dimethylaminopropyl)-N′-ethylcarbodiimide hydrochloride; PV, pervanadate; SD, standard deviation.

1. Introduction

The A Disintegrin And Metalloproteases (ADAMs) are a family of transmembrane proteins involved in cell adhesion and proteolysis. They are zinc metalloproteinases characterized by a metalloproteinase domain responsible for proteolytic activity and a disintegrin domain that interacts with integrins. Of the 21 human ADAMs, 13 have intact metalloproteinase domains with the capacity for proteolytic activity [1]. As proteases, their main substrates are the extracellular domains of other transmembrane proteins, like cytokines, growth factors, growth factor receptors and several adhesion molecules. The most studied members of the family are ADAM-10 and ADAM-17 (also known as tumour necrosis factor-α convertase, TACE) since their misregulation is involved in Alzheimer disease and carcinogenesis. Important ADAM-10 substrates include epidermal growth factor (EGF), betacellulin, Notch, and amyloid precursor protein (APP) [2]. Furthermore, MHC class I chain-related proteins A and B (MIC-A/B) and ULPBs (UL-16 binding proteins) may also be shed by ADAM-10 and/or ADAM-17 [3]. MIC-A/B and ULPBs are present on the surface of cancer cells and are able to bind NKG2D receptors, that are expressed on natural killer (NK) cells, γδ T cells and CD8+ T lymphocytes. Upon binding to the NKG2D receptor, these molecules (also called NKG2D ligands, NKG2D-L) may trigger an immune response against tumor cells expressing these ligands. In particular, this mechanism has been described in chronic lymphocytic leukemia, acute myeloid leukemia, non-Hodgkin and Hodgkin's lymphoma (HL) [4]. However, NKG2D-L can be shed by tumor cells and, in their soluble form, impair the recognition of cancer cells by T or NK cells. Moreover, soluble (s)NKG2D-L produced at the tumor site, can down regulate the expression of the NKG2D receptor on effector lymphocytes, thus contributing to tumor escape from immune recognition [5]. Proteolytic cleavage of MIC-A has been shown to depend on ADAM-10 and/or ADAM-17, which are also able to cleave ULPBs. These enzymes are highly expressed in multiple myeloma, and other tumors [6]. Furthermore, ADAM-10 overexpression by stromal and tumor cells of the lymph node microenvironment has also been recently described in HL and some non-Hodgkin lymphomas [4c]. Based on these findings, and the well documented involvement of ADAMs in

the release of the epidermal growth factor receptor (EGFR) ligands and in EGFR activation, these enzymes have been proposed as therapeutic targets for cancer [7]. In recent years, several selective ADAM inhibitors, especially against ADAM-10 and ADAM-17, have been shown to synergize with existing therapies in reducing tumor cell growth. The majority of these synthetic inhibitors use hydroxamate as the zinc-binding group (ZBG) and are designed to interact with the subsites S1'-S3' of the MMP-like catalytic site of ADAMs. Despite the debate about the feasibility of using the hydroxamic acid as ZBG in drugs due to its potential toxicity, this moiety is still present in a large number of metalloenzyme inhibitors reported in literature including those that have reached the market (such as vorinostat, a histone deacetylase inhibitor for the treatment of cancer). In fact, the importance of the inhibitor structure in determining plasma stability and toxicity has been generally recognized [8] and in particular for ADAM inhibition the presence of a hydroxamate group as ZBG is important to have a strong affinity for the enzyme [9]. One of the compounds most investigated in cancer models is INCB3619 [10] (Figure 1A), a dual inhibitor of ADAM-10 and ADAM-17 selective over MMPs, developed by Incyte Corporation. Also compound GI254023X (Figure 1A), developed by GlaxoSmithKline and reported as ADAM-10 inhibitor selective over ADAM-17, has been largely studied [11]. However, no selective synthetic ADAM-10 inhibitors have been reported so far. In this paper we describe our optimization efforts to develop selective ADAM-10 inhibitors starting from the structure of an ADAM-17 selective inhibitor recently published by us, compound **1** [12] (Figure 1B), to be used as potential agents to treat HL. In fact, an ADAM-10 selective inhibitor could present a higher efficacy and a lower toxicity than a broad spectrum ADAM inhibitor in reducing the shedding of NKG2D-L in HL cells. A structure-based approach allowed us to modify **1** and obtain the new compounds **2** and **3** (Figure 1B) able to inhibit ADAM-10 in the nanomolar range and to reduce the shedding of MIC-B and ULBP3 and the release of tumor necrosis factor (TNF)-α (another reported substrate for ADAMs) [7] in three different HL cell lines. A crystal structure of compound **3** in complex with MMP-9 was obtained and was useful for rationalizing the selectivity of compound **3** over MMPs.

FIGURE 1 HERE

2. Results and Discussion

2.1. Design of ADAM-10 selective inhibitors.

We recently reported a series of secondary sulfonamido-based hydroxamates selective for ADAM-17 over ADAM-10 and MMPs, able to reduce activated leukocyte cell adhesion molecule (ALCAM) shedding in human ovarian cancer cell lines [12]. ALCAM is expressed at the surface of epithelial ovarian cancer (EOC) cells and is released in a soluble form, sALCAM, by ADAM-17-mediated shedding. This process is important for EOC cell migratory properties and invasiveness, and can be blocked by using ADAM-17 inhibitors [13]. Among these compounds, we chose derivative **1** as starting point for a further optimization on the basis of its high selectivity over MMPs. We hypothesized that the substitution of the 3,5-dibromobenzyloxybenzene present in **1** with a group more suitable to interact with the S1' pocket of ADAM-10 catalytic site could afford compounds with an increased affinity for ADAM-10. Based on literature data [14], we designed derivative **2** (Figure 1B) bearing a 4-(4-cyano-2-methylphenyl)piperazinyl group in P1' and a benzyloxycarbonylaminopropyl chain in the α position relative to the hydroxamate (P1). A second point of intervention could be represented by the insertion of a cycle in the scaffold of **2**, as in derivative **3** (Figure 1B) bearing a thiazolidine ring in P1. Such a constrained analog could be endowed with a different orientation in the ADAM-10 catalytic site with respect to **2**.

2.2. Molecular Modeling.

In order to further support the possible activity of **3** against ADAM-10 molecular modeling studies were carried out. Presently, no experimental 3D structures of the catalytic domain of ADAM-10 have been reported; therefore, in order to analyze the possible ligand-protein key interactions a homology model of the target protein was developed. The search for the best template for modeling was carried out by choosing X-ray structures of metalloproteinases possessing a high degree of sequence similarity with ADAM-10. The human ADAM-17 proved to have the best sequence similarity with a percentage of sequence identity of 35% and, following the alignment shown in Figure SI1 (Supporting Information), a preliminary model of ADAM-10 was built and was subjected to a simulated annealing protocol by means of the Modeller program [15]. The best scored structure was analyzed, investigating in particular its backbone conformations by means of PROCHECK [16]. An analysis of the Psi/Phi Ramachandran plot of the investigated structure indicated that only residues R291 and S404 had a partial disallowed geometry (see Figure SI2 in the Supporting Information); however, these residues were far away from the zinc binding site and belong to loop regions. The so obtained protein was then subjected to 100 ns of molecular dynamics (MD) simulation (see the Experimental Section for details). As shown in Figure SI3, in the last 50 ns the system reached an apparent equilibrium since the root-mean-square deviation (rmsd)

from the initial model of all the α carbons of the protein remained approximately constant, around the value of 3.0 Å. In order to investigate a possible binding mode for compound **3**, the trajectory of the last 50 ns of the MD simulation was divided into 500 snapshots (at time intervals of 100 ps) and the compound was docked into each snapshot by means of GOLD docking software. The so obtained 500 docking results were then clusterized and a representative complex of the most populated cluster (that corresponded to about 40% of the total docking results population) was subjected to 5 ns of a QM/MM MD simulation (see the Experimental Section for details). As shown in Figure 2, the hydroxamate acted as ZBG with also the formation of H-bonds with the carboxylic portion of E384 and the backbone oxygen of G329. The thiazolidine ring acted as a rigid spacer between the zinc binding group and the sulfonyl portion that shows H-bonds with the nitrogen backbone of G329 and V327 and that allowed the insertion of the 4-(4-cyano-2-methylphenyl)piperazinyl substituent into the S1' cavity. In particular, the methyl group showed lipophilic interactions with V377 and I379, whereas the cyano group formed an H-bond with N429 that partially closed the bottom of the S1' cavity (see Figure 2). Regarding the ligand disposition, we analyzed the rmsd of the position of the ligand with respect to starting docking pose during the QM/MM simulation. As shown in Figure SI4, the ligand disposition appeared to be very stable as it showed rmsd values in the range of 0.3 – 0.8 Å.

FIGURE 2 HERE

Given the promising results of the theoretical studies, we decided to synthesize both compounds, **2** and **3**, to experimentally verify their activity.

2.3. Chemistry. Hydroxamic acids **2** and **3** were prepared following the synthetic procedure depicted in Scheme 1. Commercially available 4-fluoro-3-methylbenzonitrile was reacted with 1,4-piperazine to afford the monoarylated derivative **4** that was converted into the corresponding sulfonyl chloride **5** by sulfonation with chlorosulfonic acid followed by treatment with phosphorus pentachloride. The key intermediate **5** was then coupled with two different amino acids H-D-Orn(Z)-OH and (D)-thiazolidine-4-carboxylic acid in order to obtain sulfonamides **6** and **7**, respectively. These latter ones were converted into the corresponding hydroxamates **2** and **3** by condensation with *O*-(*tert*-butyldimethylsilyl)hydroxylamine to give the silyl intermediates and subsequent deprotection of the hydroxamate moiety with trifluoracetic acid.

Scheme 1 [a]

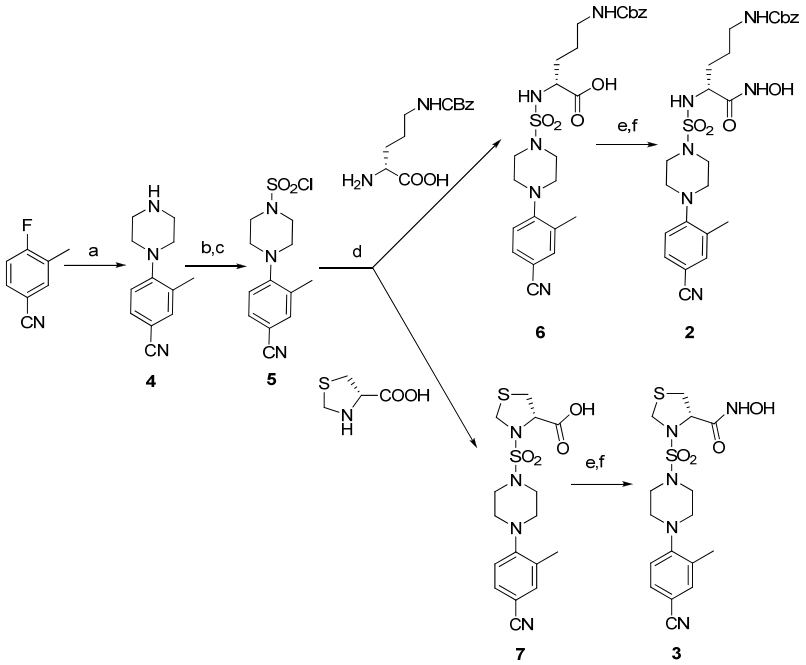

[a] Reagents: (a) piperazine, K_2CO_3, TBABr, DMSO, 100 °C, 48 h; (b) HSO_3Cl, Et_3N, CH_2Cl_2, 0 °C, then rt, 18 h; (c) PCl_5, toluene, 112 °C, 2 h; (d) H-D-Orn(Z)-OH, Et_3N, H_2O/THF, rt, 4 days, or (D)-thiazolidine-4-carboxylic acid, Et_3N, H_2O/dioxane, rt, 18 h; (e) $TBDMSiONH_2$, EDC, CH_2Cl_2, rt, 18 h; (f) CF_3COOH, CH_2Cl_2, 0 °C, then rt, 5h.

2.4. Biological Activity on Isolated Enzymes. The new hydroxamates, compounds **2** and **3**, were tested in vitro for their ability to inhibit human recombinant ADAM-10 and ADAM-17 by a fluorometric assay, which uses a fluorogenic peptide [17] as the substrate (Table 1). These compounds were compared to the previously described 3,5-dibromobenzyloxybenzene derivative **1** and to the commercial GI254023X (from now on GIX, Figure 1A). All these compounds were tested also on MMP-1, -2, -9 and -14 to evaluate their selectivity over MMPs. In particular, those MMPs most involved in carcinogenesis and tumor-induced angiogenesis were chosen (MMP-2, -9 and -14) and MMP-1, whose inhibition is commonly believed to cause some musculoskeletal side-effects associated with the administration of broad-spectrum MMP inhibitors [18]. Moreover, these enzymes were considered representative of the whole family being respectively a shallow-S1' pocket collagenase (MMP-1), two deep-S1' pocket

gelatinases (MMP-2 and -9) and a membrane bound MMP (MMP-14 or MT1-MMP), able to exert also some sheddase activities [19].

Table 1. In Vitro Enzymatic[a] Activity (IC_{50} nM values) of new compounds **2** and **3** and the reference compounds **1** and **GI254023X**.

Compd	ADAM-10	ADAM-17	MMP-1	MMP-2	MMP-9	MMP-14
3	40	1500	346000	5400	24000	100000
2	9.2	90	>200000	370	4500	50000
1	300	11	370000	1440	4400	68000
GI254023X[b]	27	860	125	2.1	5.1	88

[a] The IC_{50} values are the average of three determinations with a standard deviation of <10%. [b] Data from our lab.

The activity of GIX on isolated enzymes, previously measured and reported by using a scintillation proximity assay (SPA) [11b], was now determined by fluorimetric assay to be better compared to that of the other inhibitors. The substitution of the 3,5-dibromobenzyloxybenzene sulfonamide group of **1** with a 4-(4-cyano-2-methylphenyl)piperazine sulfonamide group as in **2** led to a shift of selectivity from ADAM-17 to ADAM-10. In fact, this change in P1' caused a 32-fold increase of activity against ADAM-10 (**2**: IC_{50}= 9.2 nM) accompanied by an 8-fold drop of activity against ADAM-17 (**2**: IC_{50}=90 nM). The selectivity for ADAM-10 over ADAM-17 was further increased by the introduction of a thiazolidine ring in P1, as in compound **3**. This derivative showed an IC_{50}= 40 nM on ADAM-10 and a 37-fold selectivity over ADAM-17 (IC_{50}= 1500 nM). Moreover, **3** was inactive against the tested MMPs (IC_{50s} > 5000 nM), thus resulting more selective than GIX over MMPs.

2.5. X-ray Crystallography.

To better elucidate the observed selectivity of compound **3** over MMPs, the crystal structure of MMP-9 in complex with **3** has been solved at 1.83 Å resolution (PDB accession code: 5CUH) with good crystallographic statistics (Supporting Information Table 1S) and with the ligand in good electron density (Figure 3A). The overall structure contains two catalytic domains of MMP-9 without the three repeats of fibronectin type II domain in the asymmetric unit. The domain consists of three α-helices, a twisted five-stranded β-sheet, eight intervening loops, including the S1′ loop that forms the S1′ deep cavity in which

compound **3** is bound (Figure 3B). The overall conformation matches well with other reported structures for MMP-9, and the position of the ligand resembles closely that observed for CC27 [20] (PDB accession code: 4H3X) (Figure 3C). The main differences that change the affinity of the two compounds for MMP-9 (IC_{50} on MMP-9: CC27= 200 nM and **3**= 24000 nM) include the twist in the six membered rings of the two ligands, the zinc chelation by the hydroxamate moieties and the position of the sulfonamide group. The two latter changes are likely to be due to the constraints imposed by the five-membered sulfur ring.

FIGURE 3 HERE

2.6. Biological Activity on HL Cell Lines. The activity of the newly synthesized ADAM-10 inhibitors **2** and **3** were evaluated in living HL cell lines (KMH2, L428 and L540) in comparison with the commercial GIX and the previously described **1**. These cell lines express MIC-B, ULBP3, the active membrane form of ADAM-10 and all, except L540, bear surface ALCAM (not shown). First, the various inhibitors were tested for toxicity on the different HL cell lines, after 72 and 96 h exposure to the various ADAM-10 inhibitors (**1**-**3** vs GIX) at 10 μM concentration, by evaluating the mitochondrial potential upon staining with the dual emission fluorescent probe JC-1. More than 96% of cell viability was found both at 72 and at 96 h after exposure to the inhibitors (not shown). Then, the ability and efficiency in decreasing the pervanadate (PV)-induced shedding of MIC-B, ULBP3 and TNFα was tested, compared to the solvent (DMSO). Each compound was assessed at 10 μM, 1 μM and 0.1 μM. As shown in Fig. 4, PV induced shedding of sMIC-B by KMH2, L428 and L540 cells was inhibited in a dose-dependent manner by **3** and **2**, with higher efficiency than **1** or GIX (IC_{50} in Table 2). This was also true for sULBP3 release (Table 2). In turn, **1**, GIX and **2** were more efficient than **3** in reducing PV induced release of sALCAM (IC_{50} in Table 2). DMSO did not exert any significant effect (shedding superimposable to that in culture medium without DMSO, not shown). These results indicate that ADAM-10 is the enzyme most involved in NKG2D-L shedding (measured as sMIC-B and sULBP3 release), while ADAM-17 is the principal enzyme responsible for the ALCAM shedding (measured as sALCAM release). Of note, all the inhibitors were also able to reduce the shedding of TNFα (IC_{50} in Table 2), a substrate for ADAMs sheddases and a reported growth factor for lymphoma cells [21]. In particular, **1** is the most efficient on TNFα inhibition, conceivably due to its higher specificity and potency for ADAM-17 (Table 1) that has been shown as the major sheddase for TNFα [6b]. The biological activity of the inhibitors on ligand shedding has IC_{50}s in the micromolar range, rather than in the nanomolar range like in the assays on isolated enzymes. This can be explained taking into account the complexity of the cell system, where

membrane-bound ADAM-10, instead of purified or recombinant molecule, is present and regulatory mechanisms occur as well.

FIGURE 4 HERE

Table 2. Cellular Activity of Synthesized compounds **2**, **3** and the Reference Compounds **1** and GI254023X.

Shedding inhibition, IC_{50} (μM)												
Compd.	KMH2				L428				L540			
	sULBP3	*sMICB*	*TNFα*	*sALCAM*	*sULBP3*	*sMICB*	*TNFα*	*sALCAM*	*sULBP3*	*sMICB*	*TNFα*	*sALCAM*
3	7	5	10	10	5	5	10	12	7	7	10	n.a.
2	10	7	10	1	10	7	12	1	10	12	10	n.a.
1	15	15	0.5	0.5	10	15	0.5	0.1	12	15	1	n.a.
GIX	10	12	10	10	15	12	5	10	10	12	7	n.a.

n.a.: not applicable as L540 is ALCAM negative (PV stimulated shedding <100pg/mL/10^5 cells).

3. Conclusions

Hodgkin's lymphoma is the most common malignant lymphoma in young people in the western world. This disease is characterized by an overexpression of ADAM-10 and increased release of NKG2D ligands, which are involved in an impaired immune response against tumor cells. Here we report our optimization efforts to develop potent and selective ADAM-10 inhibitors, starting from previously published ADAM-17 selective inhibitor **1**. Optimization of the P1' and P1 groups led to the identification of compound **3**, endowed with an improved ADAM-10 selectivity over ADAM-17 and MMPs. Molecular modeling studies suggested that the high affinity for ADAM-10 was due to the presence of the thiazolidine ring that acted as a rigid spacer between the ZBG and the sulfonyl portion of **3** and to the 4-(4-cyano-2-methylphenyl)piperazinyl group in P1'. X-ray crystal structure of **3** in complex with MMP-9 catalytic domain was used to rationalize the selectivity of **3** over MMPs. We observed that the constraints imposed by the five-membered sulfur ring led to a distorted orientation of the sulfonamide group that reduced the affinity for MMP-9 active site. These findings confirmed our starting hypothesis about the importance to properly combine structural constraints (given by a thiazolidine ring in P1) with the nature of the P1' substituent to drive ADAM-10 selectivity. **3** was tested in three different HL cell lines and was able to inhibit the shedding of NKG2D ligands in a dose-dependent manner with higher efficiency than **1**. In turn,

1 was more efficient than **3** in reducing PV induced release of sALCAM. These results suggest that ADAM-10 is the enzyme most involved in NKG2D-L shedding, while ADAM-17 is the principal enzyme responsible for the ALCAM shedding, as already known. Interestingly, the new compounds, **2** and **3**, show a significant ability to reduce the shedding of TNFα (a reported growth factor for HL cells). This opens the way to the use of selective ADAM-10 inhibitors as a part of anti-lymphoma treatment to improve the efficacy of current therapies.

4. Experimental Section

4.1. Chemistry.

Melting points were determined on a Kofler hot-stage apparatus and are uncorrected. ^{1}H and ^{13}C NMR spectra were determined with a Varian Gemini 200 MHz spectrometer or a Bruker Avance III HD 400 MHz spectrometer. Chemical shifts (δ) are reported in parts per million (ppm) and referenced according to deuterated solvent. Coupling constants *J* are reported in hertz; ^{13}C NMR and spectra were fully decoupled. The following abbreviations are used: singlet (s), doublet (d), triplet (t), double−doublet (dd), broad (brs), and multiplet (m). Chromatographic separations were performed on silica gel columns by flash column chromatography (Kieselgel 40, 0.040−0.063 mm; Merck) or using ISOLUTE Flash Si II cartridges (Biotage). Reactions were followed by thin-layer chromatography (TLC) on Merck aluminum silica gel (60 F254) sheets that were visualized under a UV lamp, and hydroxamic acids were visualized with $FeCl_3$ aqueous solution. Evaporation was performed in vacuo (rotating evaporator). Sodium sulfate was always used as the drying agent. D-Cbz-ornithine (H-D-Orn(Z)-OH) and D-thiazolidine-4-carboxylic acid were purchased from Bachem (Switzerland). 4-Fluoro-3-methylbenzonitrile was purchased from ABCR (Germany). All other commercially available chemicals were purchased from Sigma-Aldrich. Combustion analyses on target compounds were performed by our Analytical Laboratory in Pisa. All compounds showed >95% purity. Analytical results are within ±0.40% of the theoretical values.

4.2. 3-Methyl-4-(piperazin-1-yl)benzonitrile (4). To a solution of 4-fluoro-3-methylbenzonitrile (1.40 g, 10.40 mmol) in DMSO (10 mL), piperazine (2.69 g, 31.2 mmol), K_2CO_3 (2.16 g, 15.6 mmol) and TBABr (33 mg, 0.10 mmol) were added and the reaction mixture was stirred at 100 °C for 48 h. The crude was then taken up with H_2O (80 mL) and extracted with EtOAc (2 x 50 mL). The organic phase was washed with 1N HCl (2 x 50 mL); the aqueous phase was then alkalinized with 4N NaOH and extracted with EtOAc (3 x 50 mL). The organic extacts were dried over Na_2SO_4 and concentrated in vacuo to give 3-methyl-4-(piperazin-1-yl)benzonitrile as pale yellow solid (1.87 g, 90% yield). ^{1}H NMR (400 MHz, DMSO-d_6) δ: 2.31 (s, 3H), 2.36 (brs, 1H), 2.95–2.97 (m, 4H), 3.05–3.08 (m, 4H), 6.99 (d, *J*=8.2 Hz, 1H), 7.43–7.46 (m, 2H).

4.3. 4-(4-Cyano-2-methylphenyl)piperazine-1-sulfonyl chloride (5). A solution of 3-methyl-4-(piperazin-1-yl)benzonitrile (1.06 g, 5.27 mmol) and Et_3N (1.47 mL, 10.53 mmol) in dry CH_2Cl_2 (13 mL) was cooled at 0 °C and chlorosulfonic acid (0.35 mL, 5.27 mmol) was added dropwise. After the addition the mixture was allowed to reach rt and stirred for 18 h under inert atmosphere. The solvent was then removed in vacuo, the residue was triturated with Et_2O. The sulfonic acid intermediate thus obtained was suspended in dry toluene (10 mL), phosphorus pentachloride (1.09 g, 5.27 mmol) was added portionwise and the mixture was heated at 112 °C for 2 h. After cooling to rt, the reaction mixture was dissolved in EtOAc (100 mL), washed with $NaHCO_3$ ss (2 x 50 mL) and brine (1 x 80 mL). The organic phase was dried over Na_2SO_4 and evaporated in vacuo to afford a brown solid. The crude was purified by flash chromatography (*n*-hexane/EtOAc 12:1) using a Isolute Flash Si II cartridge to afford **5** as a white solid (1.05 g, 66% yield). ^{1}H NMR (400 MHz, $CDCl_3$) δ: 2.34 (s, 3H), 3.15–3.17 (m, 4H), 3.46–3.56 (m, 4H), 7.04 (d, *J*=8.9 Hz, 1H), 7.49–7.51 (m, 2H).

4.4. (*R*)-5-(Benzyloxycarbonylamino)-2-(4-(4-cyano-2-methylphenyl) piperazine-1-sulfonamido)pentanoic acid (6). To a solution of H-D-Orn(Z)-OH (270 mg, 1.00 mmol) in H_2O (10 mL) containing Et_3N (0.28 mL, 2.00 mmol), a solution of sulfonyl chloride **5** (300 mg, 1.00 mmol) in THF (10 mL) was added dropwise. The resulting mixture was stirred for 4 days at rt. The solvent was evaporated and the residue was treated with EtOAc (1 x 100 mL), washed with 1N HCl (1 x 80 mL) and brine (1 x 80 mL). The organic phase was dried over Na_2SO_4 and concentrated in vacuo. The crude product was purified by flash chromatography ($CHCl_3$/MeOH 30:1) using a Isolute Flash Si II cartridge to give **6** as a white solid (80 mg, 15% yield). ^{1}H NMR (400 MHz, DMSO-d_6) δ: 1.50–1.69 (m, 4H), 2.27 (s, 3H), 2.97–3.03 (m, 6H), 3.15–3.23 (m, 4H), 3.66–3.72 (m, 1H), 5.00 (s, 2H), 7.11 (d, *J*=8.9 Hz, 1H), 7.28–7.38 (m, 5H), 7.60–7.62 (m, 2H), 7.88 (d, *J*=9.3 Hz, 1H), 12.77 (brs, 1H).

4.5. (*R*)-Benzyl (4-(4-(4-cyano-2-methylphenyl)piperazine-1-sulfonamido)-5-(hydroxyamino)-5-oxopentyl)carbamate (2). To a suspension of carboxylic acid **6** (75 mg, 0.14 mmol) in dry CH_2Cl_2 (2.4 mL) O-(*tert*-butyldimethylsilyl)hydroxylamine (21 mg, 0.14 mmol) and EDC (41 mg, 0.21 mmol) were added. After being stirred at rt overnight, the mixture was washed with H_2O and the organic extracts were dried over Na_2SO_4 and concentrated in vacuo. The crude product was purified by flash chromatography (*n*-hexane/EtOAc 5:1) using an Isolute Flash Si II cartridge to give the *O*-silylate derivative as a pale yellow solid (40 mg, 43% yield). ^{1}H NMR (400 MHz, $CDCl_3$) δ: 0.22 (s, 6H), 0.97 (s, 9H), 1.56–1.88 (m, 4H), 2.30 (s, 3H), 2.95–3.19 (m, 6H), 3.34–3.41 (m, 4H), 3.54–3.60 (m, 1H), 5.04–5.15 (m, 3H), 7.00 (d, *J*=8.8 Hz, 1H), 7.31–7.37 (m, 5H), 7.44–7.46 (m, 2H), 9.27 (brs, 1H). To a solution of the *O*-silylate hydroxamate (40 mg, 0.061 mmol) in CH_2Cl_2 (1 mL), cooled at 0 °C, CF_3COOH (0.026 mL, 3.46 mmol)

was added dropwise. After being stirred for 1 h at 0 °C, the reaction mixture was allowed to reach rt and stirred under these reaction conditions for 4 h. The solvent was then removed in vacuo and the crude product was purified by trituration with Et_2O/*n*-hexane to give the hydroxamate **2** as a white solid (20 mg, 60% yield). Mp: 46–48 °C. ^{1}H NMR (400 MHz, DMSO-d_6) δ: 1.39–1.53 (m, 4H), 2.27 (s, 3H), 2.96–3.00 (m, 6H), 3.10–3.15 (m, 4H), 3.50–3.55 (m, 1H), 5.00 (s, 2H), 7.10 (d, *J*=9.0 Hz, 1H), 7.29–7.36 (m, 5H), 7.60–7.62 (m, 2H), 7.79 (d, *J*=9.1 Hz, 1H), 8.93 (brs, 1H), 10.66 (s, 1H). ^{13}C NMR (100 MHz, DMSO-d_6) δ: 18.28, 26.54, 30.76, 40.37, 46.10, 50.26, 54.50, 65.61, 104.98, 119.75, 120.03, 128.16, 128.20, 128.81, 131.44, 133.15, 134.96, 137.69, 155.47, 156.57, 168.47. Elemental Analysis for $C_{25}H_{32}N_6O_6S$ calculated: % C, 55.13; % H, 5.92; % N, 15.43; found: % C, 55.32; % H, 5.99; % N, 15.40.

4.6. (*S*)-3-((4-(4-Cyano-2-methylphenyl)piperazin-1-yl)sulfonyl)thiazolidine-4-carboxylic acid (7). To a solution of (D)-thiazolidine-4-carboxylic acid (243 mg, 1.83 mmol) and Et_3N (0.51 mL, 3.65 mmol) in H_2O/dioxane (2 mL/7 mL), sulfonyl chloride **5** (547 mg, 1.83 mmol) was added portionwise and the mixture was stirred at rt overnight. The dioxane was then evaporated and the residue was treated with EtOAc (1 x 100 mL), washed with 1N HCl (2 x 50mL) and brine (1 x 50 mL). The organic phase was dried over Na_2SO_4 and concentrated in vacuo. The crude was then triturated twice in $CHCl_3$/*n*-hexane to give compound **7** as a yellow powder (397 mg, 54% yield). Mp: 148–150 °C. ^{1}H NMR (200 MHz, DMSO-d_6) δ: 2.27 (s, 3H), 2.94–3.04 (m, 4H), 3.20–3.42 (m, 6H), 4.31 (d, *J*=9.5 Hz, 1H), 4.69 (d, *J*=9.5 Hz, 1H), 4.80 (dd, J_1=3.6 Hz, J_2=3.4 Hz, 1H), 7.12 (d, *J*=8.7 Hz, 1H), 7.60–7.63 (m, 2H).

4.7. (*S*)-3-((4-(4-Cyano-2-methylphenyl)piperazin-1-yl)sulfonyl)-N-hydroxythiazolidine-4-carboxamide (3). Starting from carboxylic acid **7** (271 mg, 0.685 mmol) and *O*-(*tert*-butyldimethylsilyl)hydroxylamine (215 mg, 0.685 mmol) the *O*-silylate derivative was obtained following the procedure reported for compound **2**. The crude was purified by flash chromatography (*n*-hexane/EtOAc 3:1) using a Isolute Flash Si II cartridge to afford the *O*-silylate derivative as a white solid (77 mg, 24% yield). ^{1}H NMR (200 MHz, $CDCl_3$) δ: 0.21 (s, 6H), 0.97 (s, 9H), 2.30 (s, 3H), 3.01 (t, *J*=4.7 Hz, 4H), 3.27–3.60 (m, 6H), 4.33 (d, *J*=10.2 Hz, 1H), 4.63 (dd, J_1=4.6 Hz, J_2=4.6 Hz, 1H), 4.70 (d, *J*=10.2 Hz, 1H), 6.99 (d, *J*=8.8 Hz, 1H), 7.45–7.50 (m, 2H), 8.72 (s, 1H). The *O*-silylate derivative (77 mg, 0.162 mmol) was converted in hydroxamate following the procedure reported for compound **2**. The crude product was purified by trituration with Et_2O/*n*-hexane affording **3** as a white solid (45 mg: 77% yield). Mp: 73–75 °C. ^{1}H NMR (400 MHz, DMSO-d_6) δ: 2.28 (s, 3H), 2.99 (t, *J*=4.7 Hz, 4H), 3.10 (dd, J_1=11 Hz, J_2=5.2 Hz, 1H), 3.30-3.43 (m, 5H), 4.41 (d, *J*=10.2 Hz, 1H), 4.52 (dd, J_1=5.2 Hz, J_2=5.2 Hz, 1H), 4.73 (d, *J*=10.2 Hz, 1H), 7.13 (d, *J*=8.8 Hz, 1H), 7.62–7.64 (m, 2H), 9.09 (s, 1H), 10.81 (s, 1H). ^{13}C NMR (50 MHz, $CDCl_3$) δ: 18.22, 34.97, 47.13, 51.06, 52.76, 63.70, 107.13, 119.09, 119.78, 131.22, 133.46,

135.04, 154.61, 167.80. Elemental Analysis for $C_{16}H_{21}N_5O_4S_2$, calculated: % C, 46.70; % H, 5.14; % N, 17.02; found: % C, 46.83; % H, 5.20; % N, 17.00.

4.8. MMPs and ADAMs inhibition assays.

Recombinant human MMP-14 catalytic domain was a kind gift of Prof. Gillian Murphy (Department of Oncology, University of Cambridge, UK). Pro-MMP-1, pro-MMP-2, pro-MMP-9, and recombinant human ADAM-17 (PF133) were purchased from Calbiochem. Recombinant human ADAM-10 was purchased from R&D Systems. Pro-enzymes were activated immediately prior to use with p-aminophenylmercuric acetate (APMA 2 mM for 1 h at 37 °C for MMP-2, APMA 2 mM for 2 h at 37 °C for MMP-1 and 1 mM for 1 h at 37 °C for MMP-9). For assay measurements, the inhibitor stock solutions (DMSO, 10 mM) were further diluted in the fluorometric assay buffer (FAB: Tris 50 mM, pH = 7.5, NaCl 150 mM, $CaCl_2$ 10 mM, Brij-35 0.05% and DMSO 1%). Activated enzyme (final concentration 0.56 nM for MMP-2, 1.3 nM for MMP-9, 1.0 nM for MMP-14cd, 2.0 nM for MMP-1, 5 nM for ADAM-17 and 20 nM for ADAM-10) and inhibitor solutions were incubated in the assay buffer for 3 h at 25 °C. ADAM-17 was incubated for 30 min at 37 °C and ADAM-10 for 1 h at 37 °C in a different buffer at pH = 9 (Tris 25 mM, $ZnCl_2$ 25 μM, Brij-35 0.005%). After the addition of 200 μM solution of the fluorogenic substrate Mca-Lys-Pro-Leu-Gly-Leu-Dap(Dnp)-Ala-Arg-NH_2 (Bachem) for all the enzymes in DMSO (final concentration 2 μM for all enzymes, 10 μM for ADAM-10), the hydrolysis was monitored every 15 sec for 20 min recording the increase in fluorescence (λ_{ex} = 325 nm, λ_{em} = 400 nm) with a Molecular Devices SpectraMax Gemini XPS plate reader. The assays were performed in duplicate in a total volume of 200 μL per well in 96-well microtitre plates (Corning black, NBS). Control wells lack inhibitor. The MMP inhibition activity was expressed in relative fluorescent units (RFU). Percent of inhibition was calculated from control reactions without the inhibitor. IC_{50} was determined using the formula: $v_i/v_o = 1/(1 + [I]/IC_{50})$, where v_i is the initial velocity of substrate cleavage in the presence of the inhibitor at concentration [I] and v_o is the initial velocity in the absence of the inhibitor. Results were analyzed using SoftMax Pro software and GraFit software.

4.9. Cell viability.

The Hodgkin lymphoma (HL) cell lines KMH2, L428, obtained from pleural effusion, and L540, from bone marrow of HL patients, purchased from DSMZ GmbH (Braunschweig, Germany) were used to evaluate the biological activity of ADAM-10 inhibitors. The ADAM-10 inhibitors tested (**1**-**3**) were not toxic for the different HL cell lines, after 72 and 96 h exposure at 10 μM concentration, by evaluating the

mitochondrial potential upon staining with the dual emission fluorescent probe JC-1 (Molecular Probes, Life Technologies Italia, Monza, Italy) (not shown).

4.10. ELISA for MIC-B, ULBP3, sALCAM and TNFα.

Soluble (s)MIC-B, sULBP3 and sALCAM were measured in supernatants (SN) by ELISA as described [4,12]. SN were collected from HL cell cultures before or after 24 h exposure to the various ADAM-10 inhibitors (**1**-**3**, from 10μM to 0.1μM). 100μM sodium orthovanadate was added as pervanadate (by addition of 100μM H_2O_2) for 40 min before collecting SN. The anti-ULPB3 capture mAb (M551, IgG1) was provided by Amgen (Seattle, WA). The anti-ULBP3 detection mAb (MAB15171, IgG2a) and the ELISA detection kit for sMIC-B and sALCAM were from R&D System (Minneapolis, MN). Anti-mouse IgG2a HRP was from Southern Biotechnology Associates (Birmingham, AL). Plates were developed with 2,2'azinobis(2ethylbenzothiazoline-6-sulfonic acid) (Sigma) and read at a OD_{450}nm. Results are expressed as ng/mL and referred to a standard curve obtained with the MICB/Fc or ULBP3/Fc chimeras (R&D System). TNFα was measured after treatment for 1h of each SN with 1N HCl followed by 1N NaOH with a TNFα specific kit (PeproTech EC, London, UK). Results were normalized to a standard curve and expressed as pg/mL.

4.11. Statistical analysis.

Data are presented as mean±SD. Statistical analysis was performed using two-tails student's *t* test. The cut-off value of significance is indicated in each legend to figure.

4.12. Homology Modeling.

All the primary sequences were obtained from the SWISS-PROT protein sequence database [22]. Sequence similarity searches were carried out using BlastP [23]. The crystal structure of the human ADAM-17 (2I47) was taken from the Protein Data Bank [24]. The sequence alignment was performed by CLUSTAL W [25], with a gap open penalty of 10 and a gap extension penalty of 0.05. Starting from this alignment, ten structures were generated by means of the "very slow MD annealing" refinement method, as implemented in Modeller, and the best receptor model was chosen on the basis of the DOPE (Discrete Optimized Protein Energy) assessment method. The backbone conformation of the resulting receptor structure was evaluated by inspection of the Ramachandran plot using PROCHECK. The chosen receptor model was subjected to MD simulation by means of AMBER 12 [26]. The complex was placed in a rectangular parallelepiped water box, an explicit solvent model for water, TIP3P, was used, and the complex was solvated with a 20 Å water cap. Chlorine ions were added as counterions to neutralize the system. Two steps of minimization were then carried out: in the first stage, we kept the protein fixed with

a position restraint of 500 kcal/mol•Å^2, and we solely minimized the positions of the water molecules. In the second stage, we minimized the entire system through 10000 steps of Steepest Descent followed by Conjugate Gradient (CG) until a convergence of 0.05 kcal/ Å•mol. Particle mesh Ewald (PME) [27] electrostatics and periodic boundary conditions were used in the simulation, MD trajectory was run using the minimized structure as the starting conformation, the time step of the simulations was 2.0 fs with a cutoff of 10 Å for the nonbonded interaction, and SHAKE was employed to keep all bonds involving hydrogen atoms rigid. Constant-volume periodic boundary MD was carried out for 500 ps, during which the temperature was raised from 0 to 300 K; then 99.5 ns of constant-pressure periodic boundary MD was carried out at 300 K using the Langevin thermostat to maintain constant the temperature of our system. During the first 6.5 ns, the α carbons of the receptor were blocked with a harmonic force constant of 20 kcal/mol•Å^2.

4.12. Docking studies.

We extracted from the last 50 ns of the ADAM-10 MD simulation 500 snapshots (at time intervals of 100 ps) that were used as target proteins for the docking calculations. The ligand was built by means of Maestro [28] and were then subjected to a conformational search of 1000 steps in a water environment (using the Generalized-Born/Surface-Area model) by means of Macromodel [29]. The algorithm used was the Monte Carlo method with the MMFFs and a distance-dependent dielectric constant of 1.0. The so obtained ligand was docked into the 500 ADAM-10 conformations by means of GOLD 5.1 [30]. The zinc ion was set as a trigonal bipyramidal atom; the docking program recognized the coordination of three histidines with the zinc ion, and then in order to satisfy the trigonal bipyramidal geometry the missing coordination points were used as fitting points that could bind to ligand acceptor groups. The "allow early termination" command was deactivated, while the possibility for the ligand to flip ring corners was activated. All the other parameters were used as Gold default values, and the ligands were submitted to 30 Genetic Algorithm runs. The so obtained 500 best docked conformations were then clusterized by means of the rms_analysis software of the GOLD suite (RMSD threshold of 2 Å). A representative complex of the most populated cluster was then subjected to 5 ns of a QM/MM MD simulation by means of AMBER 12. The quantum mechanics (QM) region was described by the DFTB theory [31] and contained the catalytic zinc ion, the imidazole rings of the three Histidine residues surrounding it, the Glu384 carboxylic group, and the hydroxamic acid of the ligand. In the molecular mechanics (MM) region, the parameters were the same as in the previous MD.

4.13. Crystallization of MMP9-compound 3 complex.

The wild type "mini-catalytic domain" of MMP-9 comprises residues Met109−Gly215 and Gln391−Gly444, without the additional fibronectin domains. The numbering used here for the mini-catalytic domain is consecutive from Met 109 to Gly269, without renumbering to allow for the insertion. The minidomain was expressed and refolded in *E. coli* inclusion bodies as previously described [32]. The MMP-9-compound **3** complex crystals were prepared from protein at 311 μM with AHA 120 mM and 10 mM compound **3** dissolved in 100% DMSO in a volumetric ratio of 3:1. The complex was screened for crystallization by sitting drop vapor diffusion using previously known crystallization conditions for various MMP-9 polymorphs [32] and to stimulate crystal growth of the chosen crystal form the streak seeding technique was applied [33]. The precipitant used for the crystal used in the data collection were: 40% monomethyl polyethylene glycol 5,000, 100 mM bicine at pH 7.25 grown at 20 °C in a cooled incubator. Mixed multicomponent cryoprotectant was used to soak the crystals prior to data collection [34]. The multicomponent cryoprotectant "CM22" consisted of 12.5 % diethylene glycol + 12.5 % ethylene glycol + 12.5 % MPD + 12.5 % glycerol + 12.5 % 2,3-butanediol [35] + 12.5 % DMSO + 12.5 mM 1-(3-Sulfopropyl)pyridinium betain. The final cryo-protectant in which the crystals were soaked consisted of 40% CM22, 18% monomethyl polyethylene glycol 2,000, 100 mM mixed linear buffer MMT (L-malic acid, MES, TRIS) mixed with 50% at buffer at pH 4.0 and 50% at pH 9.0. After the brief soak, the crystals were picked up with a cryoloop and flash-cooled in liquid nitrogen.

4.13.1. Data collection and refinement.

Data from a cryoprotected single crystal of the MMP-9 wt-**3** complex were collected at the SOLEIL beamline Proxima 2 [36] (Saclay, France) at 100 °K. The diffraction data was processed using XDS [37] and the useful resolution was estimated to be 1.83 Å [38]. The crystals belong to the orthorhombic space group $P2_12_12$ with cell parameters a = 74.7 Å, b = 97.8 Å, c = 43.5 Å (Table 1S). Molecular replacement was carried out with MOLREP [39] using the crystal structure of the hydroxamate based inhibitor CC27 in complex with the MMP-9 catalytic domain (4H3X) as the starting model [20]. After restrained refinement using REFMAC [40] the ligand was built with the CCP4 ligand sketcher [41] and fitted into the difference electron density (weighted Fo-Fc) calculated and displayed using COOT [42]. The coordinates and structure factors of compound **3** bound to the mini-catalytic domain of MMP-9 wild type have been deposited in the RCSB database with the access code 5CUH and ligand id LTQ for compound **3**.

4.13.2. Structure and ligand-binding.

The asymmetric unit contains two molecules of the mini-catalytic domain of MMP-9 each bound by an inhibitor molecule in good electron density. The ligands are positioned inside the catalytic site of MMP-9 stabilized by hydrogen bonds within the pocket involving main chain atoms and the side chain of the

catalytic Glu 227. The Zn atom is coordinated by three histidines (His230, His236 and His226; Fig. SI5). The ligand hydroxamate group (-NHOH) binds the molecules of Zn, with nearly the same distances in the two dimers. The distances of the two oxygens from the Zn atom are 2.1 Å and 2.4 Å (Fig. SI5), such interactions are shorter (2.1 Å and 2.2 Å) in the second domain (Chain B). Within the catalytic pocket of the MMP-9 two main chain interactions with the inhibitor are observed, with the Ala189 carbonyl group at a distance of 2.9 Å, and the amide group of Leu188 at 2.6 Å. The interaction with the Ala189 amide group at a distance of 3.5 Å is not shown because it is considered too long.

Accession code. The crystal structure data for the MMP-9 in complex with **3** have been deposited at Protein Data Bank with accession code: 5CUH.

SUPPLEMENTARY DATA

Supplementary data related to this article can be found at

AUTHOR INFORMATION

Corresponding Author

* phone, +39 050 2219562; fax, +39 050 2219605; e-mail: armando.rossello@farm.unipi.it.

Author Contributions

C.C. and E.N. contributed equally. The manuscript was written through contribution of all authors. All authors have given approval to the final version of the manuscript.

Conflict of interest

The authors declare no competing financial interest.

Acknowledgment.

This study was supported by the Italian Association for Cancer Research (AIRC IG-12759 to M.R.Z.). C.C. is recipient of a fellowship based on the same AIRC grant. We are grateful to synchrotron SOLEIL for allocation of beam time and to Drs. William Shepard and Martin Savko for assistance and advice on strategy during data collection.

References

[1] M.J. Duffy, M. Mullooly, N. O'Donovan, S. Sukor, J. Crown, A. Pierce, P.M. McGowan, The ADAMs family of proteases: new biomarkers and therapeutic targets for cancer? Clin. Proteomics. 8 (2011) 9.
[2] M.L. Moss, M. Bomar, Q. Liu, H. Sage, P. Dempsey, P.M. Lenhart, P.A. Gillispie, A. Stoeck, D. Wildeboer, J.W. Bartsch, R. Palmisano, P. Zhou, The ADAM10 prodomain is a specific inhibitor of ADAM10 proteolytic activity and inhibits cellular shedding events, J. Biol. Chem. 282 (2007) 35712-35721.

[3] a) B.K. Kaiser, D. Yim, I.T. Chow, S. Gonzales, Z. Dai, H.H. Mann, R.K. Strong, V. Groh, T. Spies, Disulphideisomerase-enabled shedding of tumor-associated NKG2D ligands, Nature 447 (2007) 482-487. b) I. Waldhauer, D. Goehlsdorf, F. Gieseke, T. Weinschenk, M. Wittenbrink, A. Ludwig, S. Stevanovic, H.G.. Rammensee, A. Steinle, Tumor-associated MICA is shed by ADAM proteases, Cancer Res. 68 (2008) 6368-6376. c) L. Fernandez-Messina, O. Ashiiru, P. Boutet, S. Agüera-González, J.N. Skepper, H.T. Reyburn, M. Valés-Gómez, Differential mechanisms of shedding of the glycosylphosphatidylinositol (GPI)-anchored NKG2D ligands, J. Biol. Chem. 285, (2010) 8543-8551.
[4] a) A. Poggi, C. Venturino, S. Catellani, M. Clavio, M. Miglino, M. Gobbi, A. Steinle, P. Ghia, S. Stella, F. Caligaris-Cappio, M.R. Zocchi, Vδ1 T lymphocytes from B-CLL patients recognize ULBP3 expressed on leukemic B cells and up-regulated by trans-retinoic acid, Cancer Res**.** 64 (2004) 9172-9179. b) S. Catellani, A. Poggi, A. Bruzzone, P. Dadati, J.L. Ravetti, M. Gobbi, M.R. Zocchi, Expansion of Vdelta1 T lymphocytes producing IL-4 in low-grade non-Hodgkin lymphomas ex pressing UL-16-binding proteins, Blood, 109 (2007) 2078-2085. c) M.R. Zocchi, S. Catellani, P. Canevali, S. Tavella, A. Garuti, B. Villaggio, A. Zunino, M. Gobbi, G. Fraternali-Orcioni, A. Kunkl, J.L. Ravetti, S. Boero, A. Musso, A. Poggi, High ERp5/ADAM10 expression in lymph node microenvironment and impaired NKG2D-ligands recognition in Hodgkin lymphomas, Blood, 119 (2012) 1479-1489.
[5] A.C. Hayday, Gammadelta T cells and the lymphoid stress-surveillance response, Immunity 31 (2009) 184-196.
[6] a) M. Jinushi, M. Vanneman, N.C. Munshi, Y.T. Tai, R.H. Prabhala, J. Ritz, D. Neuberg, K.C. Anderson, D.R. Carrasco, G. Dranoff, MIC-A antibodies and shedding are associated with the progression of multiple myeloma, Proc. Natl. Acad. Sci. USA, 105 (2008) 1285-1290. b) J. Pruessmeyer, A. Ludwig, The good, the bad and the ugly substrates for ADAM10 and ADAM17 in brain pathology, inflammation and cancer, Semin. Cell. Dev. Biol. 20 (2009) 164-174.
[7] a) G. Murphy, The ADAMs: signalling scissors in the tumour microenvironment, Nat. Rev. Cancer. 8 (2008) 929-941. b) M.J. Duffy, E. McKiernan, N. O'Donovan, P.M. McGowan, Role of ADAMs in cancer formation and progression, Clin. Cancer Res. 15 (2009) 1140-1144. c) P. Saftig, K. Reiss, The "A Disintegrin And Metalloproteases" ADAM10 and ADAM17: novel drug targets with therapeutic potential?, Eur. J. Cell Biol. 90 (2011) 527-535.
[8] a) M. Flipo, J. Charton, A. Hocine, S. Dassonneville, B. Deprez, R. Deprez-Poulain, Hydroxamates: relationships between structure and plasma stability, J. Med. Chem. 52 (2009) 6790-6802; b) J.A. Day, S.M. Cohen, Investigating the selectivity of metalloenzyme inhibitors, J. Med. Chem. 56 (2013) 7997-8007.
[9] S. DasGupta, P.R. Murumkar, R. Giridhar, M.R. Yadav, Current perspective of TACE inhibitors: a review, Bioorg. Med. Chem. 17 (2009) 444-459.
[10] a) X. Liu, J.S. Fridman, Q. Wang, E. Caulder, G. Yang, M. Covington, C. Liu, C. Marando, J. Zhuo, Y. Li, W. Yao, K. Vaddi, R.C. Newton, P.A. Scherle, S.M. Friedman, Selective inhibition of ADAM metalloproteases blocks HER-2 extracellular domain (ECD) cleavage and potentiates the anti-tumor effects of trastuzumab, Cancer Biol. Ther. 5 (2006) 648-656. b) J.S. Fridman, E. Caulder, M. Hansbury, X. Liu, G. Yang, Q. Wang, Y. Lo, B.B. Zhou, M. Pan, S.M. Thomas, J.R. Grandis, J. Zhuo, W. Yao, R.C. Newton, S.M. Friedman, P.A. Scherle, K. Vaddi, Selective inhibition of ADAM metalloproteases as a novel approach for modulating ErbB pathways in cancer, Clin. Cancer Res. 13 (2007) 1892-1902.
[11] a) R.C. Andrews, M.W. Andersen, D.J. Cowan, D.N. Deaton, S.H. Dickerson, D.H. Drewry, M.D. Gaul, M.J. Luzzio, M.H. Rabinowitz, Formamides as therapeutic agents, US Pat. Appl. US 6172064, 2001. b) C. Hundhausen, D. Misztela, T.A. Berkhout, N. Broadway, P. Saftig, K. Reiss, D. Hartmann, F. Fahrenholz, R. Postina, V. Matthews, K.J. Kallen, S. Rose-John, A. Ludwig, The disintegrin-like metalloproteinase ADAM10 is involved in constitutive cleavage of CX3CL1 (fractalkine) and regulates CX3CL1-mediated cell-cell adhesion, Blood 102 (2003) 1186-1195. c) A. Ludwig, C. Hundhausen, M.H. Lambert, N. Broadway, R.C. Andrews, D.M. Bickett, M.A. Leesnitzer, J.D. Becherer, Metalloproteinase inhibitors for the disintegrin-likemetalloproteinases ADAM10 and ADAM17 that differentially block

constitutive and phorbol esterinducible shedding of cell surface molecules, Comb. Chem. High Throughput Screen. 8 (2005) 161–171.
[12] E. Nuti, F. Casalini, S. Santamaria, M. Fabbi, G. Carbotti, S. Ferrini, L. Marinelli, V. La Pietra, E. Novellino, C. Camodeca, E. Orlandini, S. Nencetti, A. Rossello, Selective Arylsulfonamide Inhibitors of ADAM-17: Hit Optimization and Activity in Ovarian Cancer Cell Models, J. Med. Chem. 56 (2013) 8089−8103.
[13] G. Carbotti, A.M. Orengo, D. Mezzanzanica, M. Bagnoli, A. Brizzolara, L. Emionite, A. Puppo, M.G. Centurioni, M. Bruzzone, P. Marroni, A. Rossello, S. Canevari, S. Ferrini, M. Fabbi, Activated leukocyte cell adhesion molecule soluble form: a potential biomarker of epithelial ovarian cancer is increased in type II tumors, Int. J. Cancer, 132 (2013) 2597-2605.
[14] a) D.M. Burns, W. Yao, C. He, Hydroxamic acid derivatives as metalloprotease inhibitors, US Pat. Appl. US 0250789, 2005. b) D.M. Burns, C. He, Y. Li, P. Scherle, X. Liu, C.A. Marando, M.B. Covington, G. Yang, M. Pan, S. Turner, J.S. Fridman, G. Hollis, K. Vaddi, S. Yeleswaram, R. Newton, S. Friedman, B. Metcalf, W. Yao, Conversion of an MMP-potent scaffold to an MMP-selective HER-2 sheddase inhibitor via scaffold hybridization and subtle P1' permutations, Bioorg. Med. Chem. Lett. 18 (2008) 560-564.
[15] A. Fiser, R.K. Do, A. Sali, Modeling of loops in protein structures, Protein Sci. 9 (2000) 1753-1773.
[16] R.A. Laskowski, M.W. Macarthur, D.S. Moss, J.M. Thornton, Procheck - a Program to Check the Stereochemical Quality of Protein Structures, J. Appl. Crystallogr. 26 (1993) 283-291.
[17] U. Neumann, H. Kubota, K. Frei, V. Ganu, D. Leppert, Characterization of Mca-Lys-Pro-Leu-Gly-Leu-Dpa-Ala-Arg-NH2, a fluorogenic substrate with increased specificity constants for collagenases and tumor necrosis factor converting enzyme, Anal. Biochem. 328 (2004) 166–173.
[18] D.P. Becker, T.E. Barta, L.J. Bedell, T.L. Boehm, B.R. Bond, J. Carroll, C.P. Carron, G.A. Decrescenzo, A.M. Easton, J.N. Freskos, C.L. Funckes-Shippy, M. Heron, S. Hockerman, C.P. Howard, J.R. Kiefer, M.H. Li, K.J. Mathis, J.J. McDonald, P.P. Mehta, G.E. Munie, T. Sunyer, C.A. Swearingen, C.I. Villamil, D. Welsch, J.M. Williams, Y. Yu, J. Yao, Orally active MMP-1 sparing α-tetrahydropyranyl and α-piperidinyl sulfone matrix metalloproteinase (MMP) inhibitors with efficacy in cancer, arthritis, and cardiovascular disease, J. Med. Chem. 53 (2010) 6653-6680.
[19] S. Pahwa, M.J. Stawikowski, G.B. Fields, Monitoring and Inhibiting MT1-MMP during Cancer Initiation and Progression, Cancers 6 (2014) 416-435.
[20] C. Antoni, L. Vera, L. Devel, M.P. Catalani, B. Czarny, E. Cassar-Lajeunesse, E. Nuti, A. Rossello, V. Dive, E.A. Stura, Crystallization of bi-functional ligand protein complexes, J. Struct. Biol. 182 (2013) 246-254.
[21] S. Nakayama, T. Yokote, M. Tsuji, T. Akioka, T. Miyoshi, Y. Hirata, N. Hiraoka, K. Iwaki, A. Takayama, U. Nishiwaki, Y. Masuda, T. Hanafusa, Expression of tumour necrosis factor-α and its receptors in Hodgkin lymphoma, Br. J. Haematol. 167 (2014) 574-577.
[22] E. Gasteiger, A. Gattiker, C. Hoogland, I. Ivanyi, R.D. Appel, A. Bairoch, ExPASy: The proteomics server for in-depth protein knowledge and analysis, Nucleic Acids Res. 31 (2003) 3784-3788.
[23] S.F. Altschul, T.L. Madden, A.A. Schaffer, J. Zhang, Z. Zhang, W. Miller, D.J. Lipman, Gapped BLAST and PSI-BLAST: a new generation of protein database search programs, Nucleic Acids Res. 25 (1997) 3389-3402.
[24] a) J.S. Condon, D. Joseph-McCarthy, J.L. Levin, H.G. Lombart, F.E. Lovering, L. Sun, W. Wang, W. Xu, Y. Zhang, Identification of potent and selective TACE inhibitors via the S1 pocket, Bioorg. Med. Chem. Lett. 17 (2007) 34-39. b) H.M. Berman, J. Westbrook, Z. Feng, G. Gilliland, T.N. Bhat, H. Weissig, I.N. Shindyalov, P.E. Bourne, The Protein Data Bank, Nucleic Acids Res. 28 (2000) 235-242.
[25] J.D. Thompson, D.G. Higgins, T.J. Gibson, CLUSTAL W: improving the sensitivity of progressive multiple sequence alignment through sequence weighting, position-specific gap penalties and weight matrix choice, Nucleic Acids Res. 22 (1994) 4673-4680.

[26] D.A. Case, T.A. Darden, T.E. Cheatham, III, C.L. Simmerling, J. Wang, R.E. Duke, R. Luo, R.C. Walker, W. Zhang, K.M. Merz, B. Roberts, S. Hayik, A. Roitberg, G. Seabra, J. Swails, A.W. Götz, I. Kolossváry, K.F. Wong, F. Paesani, J. Vanicek, R.M. Wolf, J. Liu, X. Wu, S.R. Brozell, T. Steinbrecher, H. Gohlke, Q. Cai, X. Ye, J. Wang, M.-J. Hsieh, G. Cui, D.R. Roe, D.H. Mathews, M.G. Seetin, R. Salomon-Ferrer, C. Sagui, V. Babin, T. Luchko, S. Gusarov, A. Kovalenko, and P.A. Kollman (2012), AMBER 12, University of California, San Francisco.
[27] U. Essmann, L. Perera, M.L. Berkowitz, T. Darden, H. Lee, L.G. Pedersen, A smooth particle mesh Ewald method, J. Chem. Phys. 103 (1995) 8577-8592.
[28] Maestro, version 9.0;. Schrödinger Inc: Portland, OR, 2009.
[29] Macromodel, version 9.7; Schrödinger Inc: Portland, OR, 2009.
[30] M.L. Verdonk, J.C. Cole, M.J. Hartshorn, C.W. Murray, R.D. Taylor, Improved protein-ligand docking using GOLD, Proteins 52 (2003) 609-623.
[31] G. Seifert, D. Porezag, T. Frauenheim, Calculations of molecules, clusters, and solids with a simplified LCAO-DFT-LDA scheme, Int. J. Quantum Chem. 58 (1996) 185−192.
[32] L. Vera, C. Antoni, L. Devel, B. Czarny, E. Cassar-Lajeunesse, A. Rossello, V. Dive, E.A. Stura, Screening Using Polymorphs for the Crystallization of Protein–Ligand Complexes, Cryst. Growth Des. 13 (2013) 1878-1888.
[33] E.A. Stura, I.A. Wilson, Applications of the streak seeding technique in protein crystallization, J. Cryst. Growth 110 (1991) 270–282.
[34] L. Vera, E.A. Stura, Strategies for Protein Cryocrystallography, Cryst. Growth Des. 14 (2014) 427-435.
[35] L. Ciccone, L. Vera, L. Tepshi, L. Rosalia, A. Rossello, E.A. Stura, Multicomponent mixtures for cryoprotection and ligand solubilization, Biotechnology Reports 7 (2015) 120–127.
[36] D. Duran, S. Le Couster, K. Desjardins, A. Delmotte, G. Fox, R. Meijers, T. Moreno, M. Savko, W. Shepard, PROXIMA 2A – A New Fully Tunable Micro-focus Beamline for Macromolecular Crystallography, Journal of Physics: Conference Series, 425, 012005.
[37] W. Kabsch, XDS, Acta Crystallogr. D. Biol. Crystallogr. 66 (2010) 125–132.
[38] K. Diederichs, P.A. Karplus, Improved R-Factors for Diffraction Data Analysis in Macromolecular Crystallography, Nat. Struct. Biol. 4 (1997) 269–275.
[39] A. Vagin, A. Teplyakov, Molecular replacement with MOLREP, Acta Crystallogr. D Biol. Crystallogr. 66 (2010) 22–25.
[40] G.N. Murshudov, P. Skubák, A.A. Lebedev, N.S. Pannu, R.A. Steiner, R.A. Nicholls, M.D. Winn, F. Long, A.A. Vagin, REFMAC5 for the refinement of macromolecular crystal structures, Acta Crystallogr. D. Biol. Crystallogr. 67 (2011) 355–367.
[41] M.D. Winn, C.C. Ballard, K.D. Cowtan, E.J. Dodson, P. Emsley, P.R. Evans, R.M. Keegan, E.B. Krissinel, A.G.W. Leslie, A. McCoy, S.J. McNicholas, G.N. Murshudov, N.S. Pannu, E.A. Potterton, H.R. Powell, R.J. Read, A. Vagin, K.S. Wilson, Overview of the CCP4 suite and current developments, Acta Crystallogr. D. Biol. Crystallogr. 67 (2011) 235–242.
[42] P. Emsley, B. Lohkamp, W.G. Scott, K. Cowtan, Features and development of Coot, Acta Crystallogr. D Biol. Crystallogr. 66 (2010) 486–501.

Figure Captions.

Figure 1. A) Chemical structures of known ADAM-10 inhibitors. B) Design of the novel ADAM-10 selective inhibitors.

Figure 2. Compound **3** complexed with *h*ADAM-10.

Figure 3: Stick representations of the binding of **3** in the S1' cavity of MMP-9. (A). The electron-density for compound **3** (PDB accession code: 5CUH) is unambiguous, the ligand is positioned with the hydroxamate ZBG chelating the metal atom in the binding site delimited by the αB-helix at the back, the βIV-strand at the top and by the specificity loop that forges the S1' cavity shown in (B). (C). The overall position is easily predicted from the structure of CC27 (PDB accession code: 4H3X). The crystal structure provides the fine details of the changes that result from the chemical constraints imposed by the five-membered ring.

Figure 4. Dose-dependent reduction of MIC-B shedding by ADAM-10 inhibitors. Soluble (s)MIC-B was measured by ELISA in supernatants (SN) collected from KMH2 (A) or L428 (B) or L540 (C) cell cultures before or after 24 h exposure to the various ADAM-10 inhibitors (**1**, GIX, **2** and **3**, from 10 μM to 0.1 μM). 100 μM sodium orthovanadate was added as PV (by addition of 100 μM H_2O_2) for 40 min before collecting SN. The assay was performed in triplicate. The amount of sMIC-B found in SN treated with solvent (DMSO) and PV (black column) was used as 100% shedding control. Results are expressed as ng/mL referred to a standard curve obtained with the MIC-B/Fc chimera and are the mean±SD from of 3 independent experiments. *$p<0.0001$ vs DMSO; °$p<0.002$ vs DMSO.

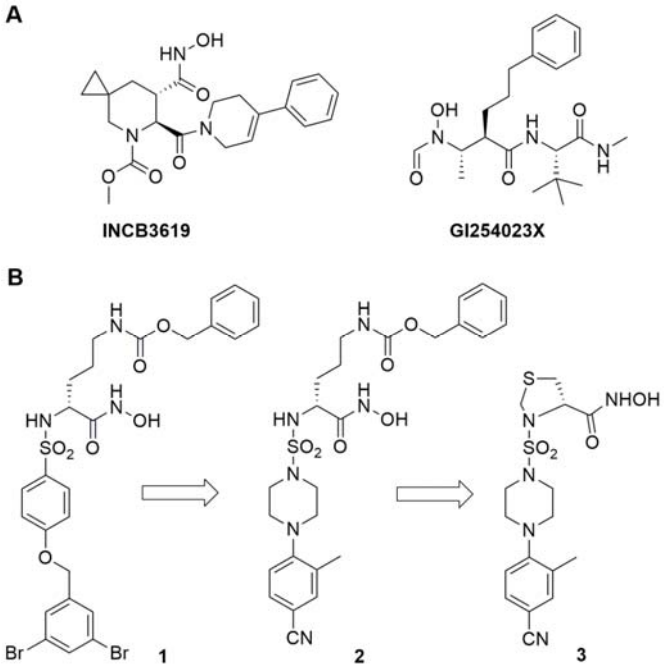

Figure 1

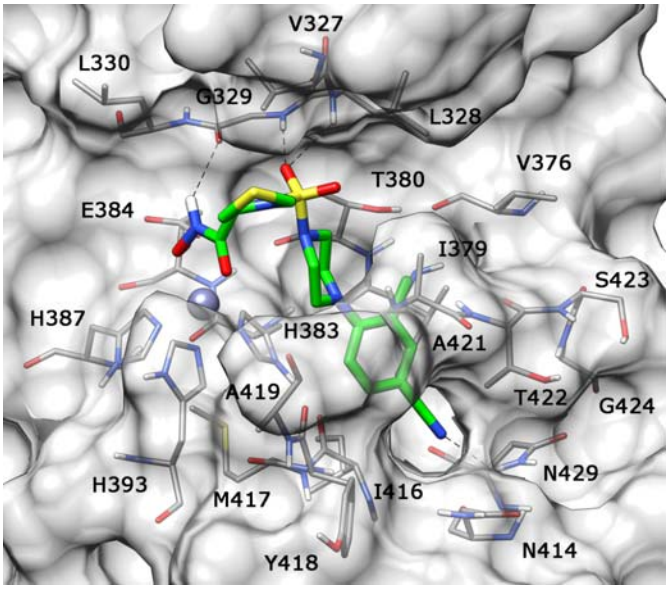

Figure 2

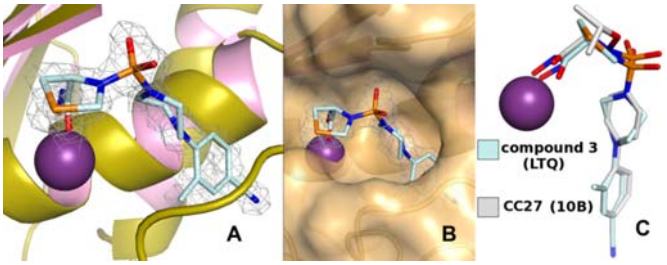

Figure 3

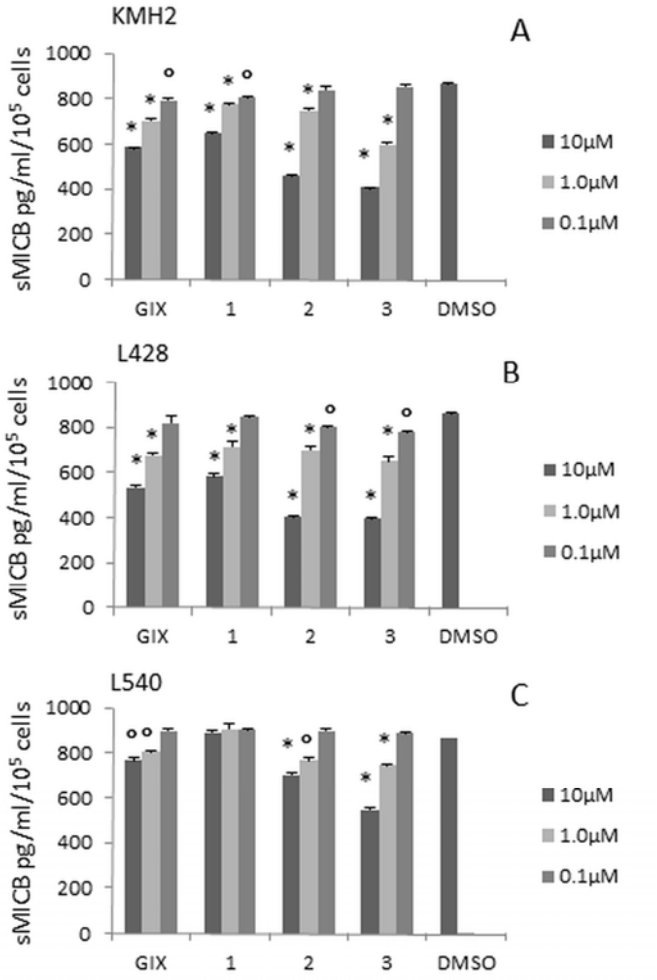

Figure 4